JOURNAL OF VIROLOGY, Jan. 2005, p. 277–288 Vol. 79, No. 1
0022-538X/05/$08.00+0 doi:10.1128/JVI.79.1.277–288.2005
Copyright © 2005, American Society for Microbiology. All Rights Reserved.

Crystal Structure of Complete Rhinovirus RNA Polymerase Suggests Front Loading of Protein Primer

Todd C. Appleby,[1] Hartmut Luecke,[2] Jae Hoon Shim,[1] Jim Z. Wu,[1] I. Wayne Cheney,[1] Weidong Zhong,[1] Lutz Vogeley,[2] Zhi Hong,[1] and Nanhua Yao[1]*

Valeant Pharmaceuticals International, Costa Mesa,[1] and Department of Molecular Biology and Biochemistry, University of California at Irvine, Irvine,[2] California

Received 28 May 2004/Accepted 8 August 2004

Picornaviruses utilize virally encoded RNA polymerase and a uridylylated protein primer to ensure replication of the entire viral genome. The molecular details of this mechanism are not well understood due to the lack of structural information. We report the crystal structure of human rhinovirus 16 3D RNA-dependent RNA polymerase (HRV16 $3D^{pol}$) at a 2.4-Å resolution, representing the first complete polymerase structure from the *Picornaviridae* family. HRV16 $3D^{pol}$ shares the canonical features of other known polymerase structures and contains an N-terminal region that tethers the *fingers* and *thumb* subdomains, forming a completely encircled active site cavity which is accessible through a small tunnel on the backside of the molecule. The small *thumb* subdomain contributes to the formation of a large cleft on the front face of the polymerase which also leads to the active site. The cleft appears large enough to accommodate a template:primer duplex during RNA elongation or a protein primer during the uridylylation stage of replication initiation. Based on the structural features of HRV16 $3D^{po1}$ and the catalytic mechanism known for all polymerases, a front-loading model for uridylylation is proposed.

Rhinovirus infections are the leading cause of the common cold (35). There are over 100 serotypes of human rhinovirus (HRV), the majority of which utilize intercellular adhesion molecule 1 as their host-cell receptor. HRV serotype 16 (HRV16) from this major receptor group is a suitable virus for clinical study (26) and can serve as a model for studying the transmission of colds and virus-induced asthma (6). Rhinoviruses are positive-strand, nonenveloped RNA viruses and are members of the *Picornaviridae* family, which comprise one of the largest families of viral pathogens responsible for many serious human and animal diseases including the common cold, hepatitis, poliomyelitis, and foot-and-mouth disease.

HRV16 contains a genome comprised of 7,124 nucleotides and includes a 5′ nontranslated region, a single open reading frame, a 3′ nontranslated region, and a poly(A) tail of approximately 40 nucleotides. The open reading frame encodes a single polyprotein of 2,152 residues (N-VP4-VP2-VP3-VP1-2A-2B-2C-3A-3B-3C-3D-C) that is cleaved by both host and viral proteases to yield the structural and nonstructural proteins of the virus (26). Among the functionally identified viral proteins are $3C^{pro}$, a cysteine protease, and $3D^{pol}$, an RNA-dependent RNA polymerase (RdRp) (27). HRV16 $3D^{pol}$ is located at the carboxy-terminal end of the polyprotein and is the core enzyme utilized for both negative-strand RNA synthesis and reiterative synthesis of multiple copies of positive-strand RNA for packaging into progeny virions (21). Rhinoviruses are very similar to poliovirus (PV), another member of the *Picornaviridae* family, in terms of genome organization, polyprotein processing, and viral protein function (42).

All classes of polymerases consist of three major subdomains (fingers, palm, and thumb) which adopt the shape of a cupped right hand (48). RdRp crystal structures from several families of viruses have been determined, including those from PV (15) (*Picornaviridae* family); from hepatitis C virus (HCV) (1, 4, 28) and bovine viral diarrhea virus (BVDV) (9) (*Flaviviridae* family); from rabbit hemorrhagic disease virus (RHDV) (36) and Norwalk virus (NV) (37) (*Caliciviridae* family); and from the double-stranded RNA bacteriophage, Φ6 (5). HCV NS5B and the Φ6 RdRp are large compared to the other known viral polymerases and contain 591 and 664 residues, respectively. The RdRps from the caliciviruses, RHDV and NV, are slightly smaller and contain about 516 and 510 residues, respectively. With 460 residues, HRV16 $3D^{pol}$ represents the smallest, fully functional RdRp known to date. The PV $3D^{pol}$, comprised of 461 residues, is very similar to HRV16 $3D^{pol}$ in size; however, the crystal structure of PV $3D^{pol}$ as currently known is missing about one-third of the molecule (15). Despite the variation in size, one feature common to all known viral RdRps is a fully encircled active site. In addition, a functional oligomeric form of PV $3D^{pol}$ has been proposed, based in part on the crystal packing of the polymerase molecules (15, 18, 30).

The ability of viruses with linear genomes to faithfully replicate their terminal ends is essential. RNA viruses that rely on RdRps for replication have evolved elegant mechanisms for performing such a critical task. In the case of HCV, NS5B contains a large thumb subdomain with a β-hairpin extension (1, 4, 28). Evidence is mounting which suggests that the β-hairpin, possibly with help from the C-terminal region of the protein, forms a scaffold upon which a 3′ terminal initiation complex can assemble (19, 38). A similar de novo initiation mechanism involving an extensive thumb subdomain and C-terminal region has been proposed for the RdRp from bacteriophage Φ6 (5, 25). For PV, RHDV, and HRV, however, a different mechanism is employed in which a small viral peptide,

* Corresponding author. Mailing address: Valeant Pharmaceuticals International, 3300 Hyland Ave., Costa Mesa, CA 92626. Phone: (714) 545-0100, ext. 2184. Fax: (714) 668-3142. E-mail: nyao@valeant.com.

TABLE 1. Summary of diffraction data

Type of data	Data by collection method (beam line)	
	Se Peak λ SAD (CHESS F2)	Se Peak λ MAD (SLS X06S)
Resolutions (wavelength) (Å)	2.6 (0.97895)	2.4 (0.97887)
No. of observations (no. of unique observations)	506,443 (76,017)	439,315 (98,759)
Completeness overall (outermost shell) (%)	98.4 (92.4)	99.8 (99.8)
R_{sym} overall (outermost shell) (%)	8.8 (35.7)	9.0 (46.3)
Average I/σ_1 overall (outermost shell)	21.3 (3.7)	12.9 (3.0)

VPg (3B), plays a critical role as a protein primer in the terminal initiation of RNA synthesis (32, 40, 41, 52). In the case of PV, the polymerase binds directly to VPg and utilizes a stem-loop *cis*-acting replication element (CRE) as a template to uridylylate a tyrosine residue near the N terminus of the small peptide (40, 41, 43). This product, VPg-pU, is subsequently extended by at least one more uridine nucleotide to give VPg-pUpU. The uridylylated VPg can then be used as a primer to initiate negative-strand RNA synthesis at the 3′ end of the genome which is polyadenylated. HRV16 $3D^{pol}$ plays a similar role in VPg uridylylation during HRV replication. In fact, it has been demonstrated that a PV/HRV-VPg chimeric virus is viable in cell culture (8). Few structural details are known, however, about the precise molecular mechanism behind VPg uridylylation.

Rhinoviruses are important targets for therapies directed against the common cold. The crystal structure of the whole virus, extensively studied by Rossmann et al. (44), aided in the development of fatty acid-like compounds (pocket factor) that disrupt the fusion of HRV with the host cell (14). These compounds can potentially be effective against the entire family of picornaviruses. The compound AG7088 (Pfizer, Inc.) directly targets HRV $3C^{pro}$ (33) and displays activity against clinical isolates of human rhinovirus (24). All commercially available cold medicines are for the relief of cold symptoms, as there are currently no direct antirhinovirus agents approved. HRV16 $3D^{pol}$ is a valid target for antirhinovirus therapy.

MATERIALS AND METHODS

Protein production and crystallization. The preparation of plasmids and protein utilized in this study has been previously described (8). Briefly, the expression construct was designed and expressed such that the resulting HRV16 $3D^{pol}$ protein contains the naturally occurring glycine residue at the amino terminus (N terminus) and a six-histidine carboxy-terminal (C-terminal) tag. Selenomethionyl-HRV16 $3D^{pol}$ (SeMet-HRV16 $3D^{pol}$) was produced in methionine auxotroph cells that were grown in the presence of seleno-L-methionine in M9 minimal salts media. Purified SeMet-HRV16 $3D^{pol}$ is concentrated to approximately 20 mg/ml in the presence of a 250 mM concentration of the nondenaturing solubilizing agent, dimethylbenzylammonium propane sulfonate (DMBAPS).

Diffraction-quality crystals are grown at room temperature by using the sitting-drop vapor diffusion technique. Typically, 2 μl of protein solution is mixed with 0.5 μl of 1.33 M DMBAPS and 2 μl of reservoir solution consisting of 40% (wt/vol) polyethylene glycol 4000, 100 mM sodium citrate (pH 5.6), 35 mM ammonium sulfate, 5% glycerol, and 5 mM dithiothreitol. After approximately 3 days, SeMet-HRV16 $3D^{pol}$ crystals appear and continue to grow for an additional 7 to 10 days. Crystals harvested directly from the sitting drops and frozen in liquid nitrogen diffract up to a 2.4-Å resolution. HRV16 $3D^{pol}$ crystals are of the monoclinic space group $P2_1$ with cell dimensions of $a = 59.4$, $b = 118.9$, and $c = 183.1$ Å and $\beta = 96.1°$, and they contain four molecules in the asymmetric unit (ASU).

X-ray diffraction data collection and structure determination. A complete single-wavelength anomalous dispersion (SAD) data set was collected on a single frozen (−180°C) SeMet-HRV16 $3D^{pol}$ crystal on the F2 beam line at the Cornell High Energy Synchrotron Source, Cornell University (Ithaca, N.Y.). The data were collected on a Quantum-210 CCD detector (ADSC, San Diego, Calif.) by using 1° scans with 2-min exposures. Bijvoet pairs were acquired by collecting the data in 18° wedges simulating inverse beam geometry. The diffraction data were processed with the program DENZO and SCALEPACK (HKL Research Inc., Charlottesville, Va.) (Table 1). Anomalous differences were calculated with the DREAR package (3), and a total of 38 of the 40 possible Se atom sites were found by SnB (50). By utilizing the top 14 Se sites as input for the program FINDNCS (29) in the CCP4 suite (10), a noncrystallographic twofold symmetry axis was identified between molecules A and B in the ASU. Molecules C and D were identified manually from the remaining Se sites. The positions and anomalous occupancies of the 38 Se atoms were refined by using the MLPHARE program (39), and the phases were improved by solvent flattening by using the program DM (11). The correct hand for the Se atom model was determined by inspecting the electron density map. The initial figure of merit for all reflections out to a resolution of 2.6 Å was 0.15 and improved to 0.50 after density modification. Utilizing the available fourfold noncrystallographic symmetry averaging in conjunction with solvent flattening resulted in a final figure of merit of 0.77. This averaged experimental map was of excellent quality, showing clear electron density for main chain and side chain atoms (Fig. 1A) as well as several solvent molecules.

By utilizing this map and the interactive graphics program, O (23), a continuous Cα trace was generated for molecule A, followed by the addition of main chain and side chain atoms. Molecules B, C, and D were generated by noncrystallographic symmetry transformations obtained from the Se sites associated with each molecule. After rigid-body refinement and one round of torsion angle annealing in CNX (Accelrys, San Diego, Calif.), the *R* factor dropped to 28% with a free *R* factor of 34% by using data to a 2.6-Å resolution. The model was then further refined against a 2.4-Å data set by using iterative cycles of torsion angle annealing and manual refitting of the model. After the data were extended to 2.4 Å, water molecules were included during subsequent rounds of refinement. Four sulfate ions and one molecule of DMBAPS (associated with molecule A) were eventually added to the final model after an inspection of difference density maps and based on potential hydrogen bonding to nearby protein atoms. Ammonium sulfate and DMBAPS are both components of the crystallization mixture. Statistics for the final model are shown in Table 2.

The HRV16 $3D^{pol}$ structure was also independently solved by molecular replacement by using X-ray diffraction data collected at the Swiss Light Source, Paul Scherrer Institut (Villigen, Switzerland) (Table 1). The partial PV $3D^{pol}$ structure (Protein Data Bank [PDB] code 1RDR) (15) was chosen as a template for the search model, which was constructed by threading the HRV16 $3D^{pol}$ sequence onto the coordinates of PV $3D^{pol}$ by utilizing the SWISS-MODEL server (45). Rotation and translation searches, performed with CNX, gave unambiguous results, allowing us to locate all four monomers in the ASU. The refined structure resulting from molecular replacement agrees extremely well with, and therefore validates, the structure determined independently by SAD phasing.

Hypothetical substrate models. The coordinates of the human immunodeficiency virus reverse transcriptase (HIV RT) ternary complex (PDB code 1RTD) (20), containing a DNA template-primer duplex, a 2′deoxythymidine-5′ triphosphate (dTTP) nucleotide, and magnesium ions, were roughly aligned with the HRV16 $3D^{pol}$ structure by using selected residues from the highly conserved palm subdomain and the LSQ_EXPLICIT routine in the program O. The template-primer duplex and the dTTP were then manually adjusted together as a rigid body in order to improve the position of the metal ions with respect to the catalytic aspartic acid residue, Asp 327 of HRV16 $3D^{pol}$. No energy minimization steps were performed to further improve the model. Other than the rigid-body alignment, the only modifications performed on the substrate model include changing the dTTP nucleotide to UTP by removing the

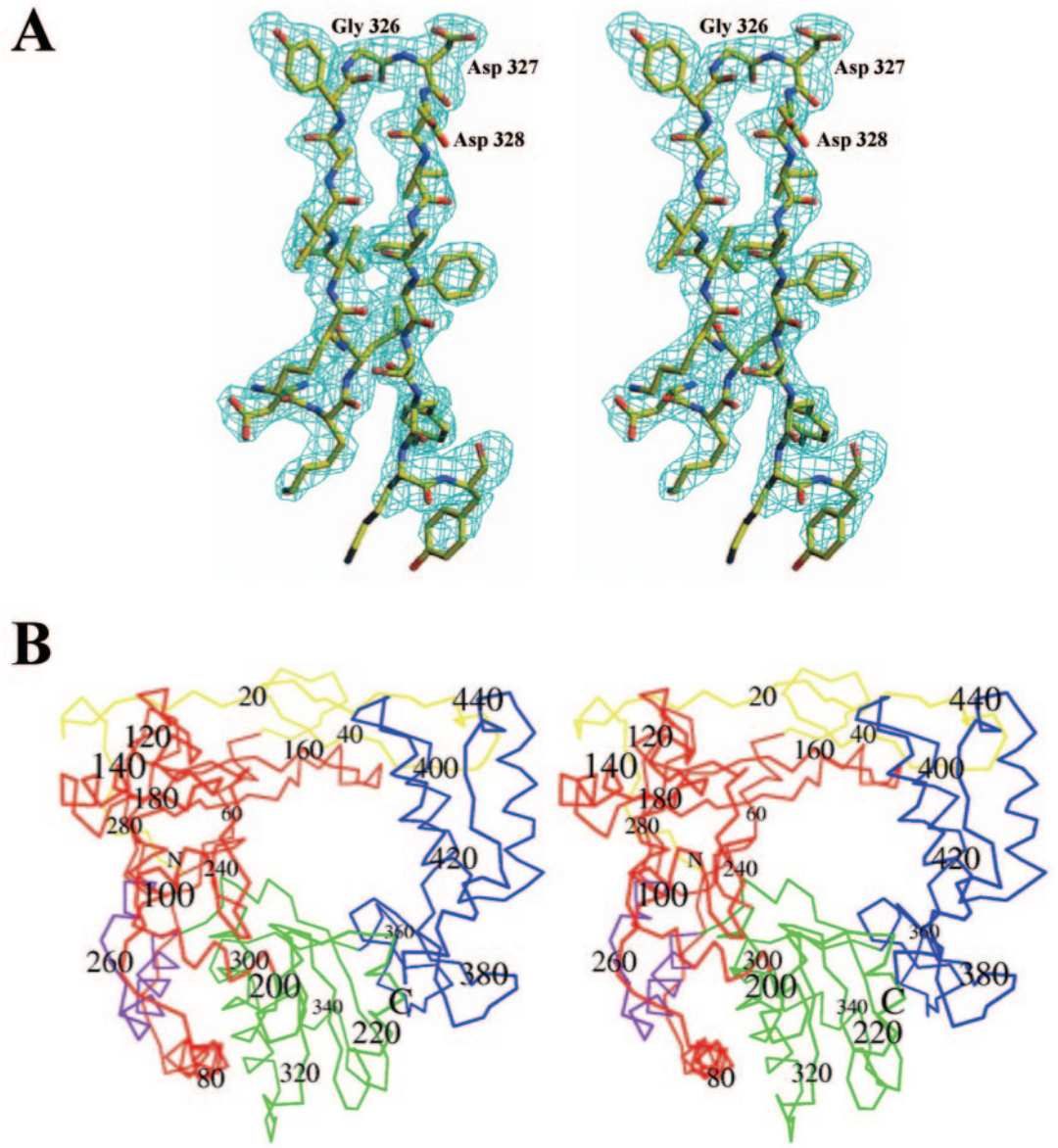

FIG. 1. (A) The averaged, solvent-flattened 2.6-Å electron density map calculated by using SAD phases and then superimposed on the final model in the region of motif C. The conserved Gly-Asp-Asp sequence is labeled. (B) A stereoview of the Cα trace for HRV16 $3D^{pol}$. The color of the trace corresponds to the N-terminal region (yellow), the fingers subdomain (red), the fingers insertion (purple), the palm subdomain (green), and the thumb subdomain (blue). N and C termini as well as every 20th residue are labeled accordingly.

5-methyl group from the thymine base and adding a 3′ hydroxyl group to the sugar moiety, as well as adding a 2′ hydroxyl group to the guanine nucleotide at the 3′ end of the primer strand. The only adjustment made to the HRV16 $3D^{pol}$ structure for this model was an approximate 120° rotation of the χ^1 torsion angle of Ser 287 in order to orient the side chain hydroxyl group towards the active site.

The schematic model for CRE and HRV16 VPg were generated by using the program InsightII (Accelrys). The coordinates used to generate the CRE were simply taken from the template strand of the HRV16 $3D^{pol}$ substrate model (see above). A few additional residues were added indiscriminately to the 3′ and 5′ ends of the template strand in order to convey a stem-loop-type structure. The coordinates used to generate the VPg-like peptide were taken from a 13-residue polyalanine model with the residues in an extended conformation. The third residue from the N terminus was mutated to a tyrosine residue in order to mimic Tyr 3 from the actual HRV16 $3D^{pol}$-VPg. The model of the uridylylation complex is intended to demonstrate only the proposed relative positions of substrates (RNA, VPg, and UTP) in the polymerase active site during VPg uridylylation and is not meant to imply the exact position of specific residues.

PDB accession number. The refined atomic coordinates (accession code 1TP7) have been deposited in the PDB, Research Collaboratory for Structural Bioinformatics, Rutgers University, New Brunswick, N.J. (http://www.rcsb.org/).

RESULTS AND DISCUSSION

Quality of the model and structural overview. The ASU of the HRV16 $3D^{pol}$ crystals contains four complete polymerase molecules (molecules A, B, C, and D). Molecules A and B are related by a noncrystallographic twofold rotation axis, while molecules C and D are not related to any other molecule in the ASU by proper noncrystallographic symmetry. All four molecules are structurally very similar, with the largest difference

TABLE 2. Crystallographic data and refinement statistics[a]

Parameter	Space group $P2_1$
Cell dimension	
a (Å)	59.4
b (Å)	118.8
c (Å)	183.1
β (°)	96.1
Resolution range (Å)	30–2.4
No. of protein atoms	14,744
No. of ligand atoms	37
No. of water molecules	270
R factor (free *R* factor) (%)	24.3 (29.2)
rms bond (Å)	0.007
rms angle (°)	1.05
Average β factors (Å^2)	
Protein main chain (side chain)	
Molecule A	48.6 (49.9)
Molecule B	57.2 (58.1)
Molecule C	74.9 (75.7)
Molecule D	79.9 (80.2)
Sulfate and DMBAPS	51.0
Water molecules	37.3

[a] rms, root mean square.

occurring between molecules B and D, which reveal a root mean square deviation (rmsd) of 0.8 Å for 460 superimposed Cα atoms. Molecules A and B have significantly lower overall *B* factors (48.6 and 57.2 Å^2, respectively) compared to molecules C and D (74.9 and 79.9 Å^2, respectively). The observed differences between the four molecules in the ASU are most likely a result of variations in the local packing environments of these molecules in the crystal and may indicate some inherent flexibility in certain regions of HRV16 3D^{pol}. The significance of the HRV16 3D^{pol} crystal packing will be discussed below (see "Comparisons to PV 3D^{pol}" below).

The averaged, solvent-flattened electron density map calculated by using SAD phases reveals continuous density from residues 1 to 460 of HRV16 3D^{pol}. The six-histidine residues which comprise the C-terminal histidine tag are not visible in the density map, most likely due to disorder. The map was of sufficient quality to reveal a majority of the side chain atoms including those of several putative active site residues (Fig. 1A). The final model contains residues 1 to 460 for all four molecules in the ASU, four sulfate ions, 270 water molecules, and a single, well-ordered molecule of the nondenaturing solubilizing agent, DMBAPS. Ramachandran analysis reveals that 99.8% of the residues are located in the allowed regions of the plot, while the remaining four residues are found in the generously allowed regions. The *R* factor of the present model is 24% with a free *R* factor of 29% (Table 2).

HRV16 3D^{pol} is a globular protein with dimensions 54 by 54 by 44 Å. The overall fold (Fig. 1B) resembles the well-characterized right-hand model containing the fingers, palm, and thumb subdomains observed in several other known polymerase structures. The N-terminal residues of HRV16 3D^{pol} span the top of the polymerase molecule, tethering together the fingers and thumb subdomains. This arrangement of structural elements creates a fully encircled active site similar to the sites observed in other viral RdRp structures such as PV 3D^{pol} (15), RHDV RdRp (36), NV RdRp (37), Φ6 RdRp (5), HCV NS5B (1, 4, 28), and the recently determined BVDV RdRp (9) (Fig. 2). The active site cavity of HRV16 3D^{pol} is accessible through a small tunnel on the back side of the molecule (see Fig. 5A), as well as through a large, central cleft approximately 14 Å across and 22 Å deep located in the front of the polymerase (Fig. 3A).

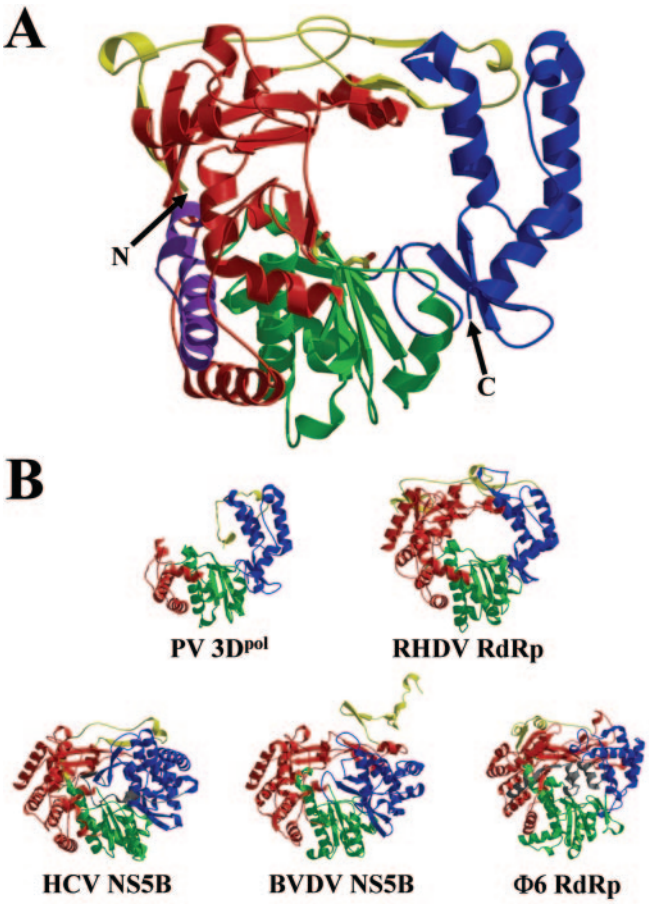

FIG. 2. (A) A ribbon representation of HRV16 3D^{pol}. Flat coils (α-helices), arrows (β-strands), and thin round coils (turns and loops) indicate secondary structural elements. The ribbon is colored according to scheme described in the legend of Fig. 1B. Catalytic Asp residues 327 and 328 are shown as stick models, while N and C termini are labeled accordingly. (B) Viral RdRp homology. The structures of PV 3D^{pol} (residues 12 to 37, 67 to 97, 181 to 266, and 291 to 461), RHDV RdRp, HCV NS5B, BVDV NS5B, and the bacteriophage Φ6 RdRp are shown in ribbon representations and colored by region based the scheme described in the legend of Fig. 1B.

N-terminal region. The HRV16 3D^{pol} N-terminal region (residues 1 to 53) forms a web that connects the fingers and thumb subdomains. The N terminus (Gly 1) of HRV16 3D^{pol} is visible in the SAD electron density map and reveals the amino group projecting into the molecule, where it hydrogen bonds with the carbonyl oxygen of Gly 240, anchoring the N terminus to the interface between the fingers and palm subdomains. The first strand of the five-stranded mixed β-sheet located in the core of the fingers subdomain is actually contributed by residues 2 to 8 of the N-terminal region. Residues 9 to 40 extend along the top surface of the fingers subdomain and loop around the tip of the thumb subdomain, forming extensive hydrophobic interactions (Fig. 3A). The N-terminal seg-

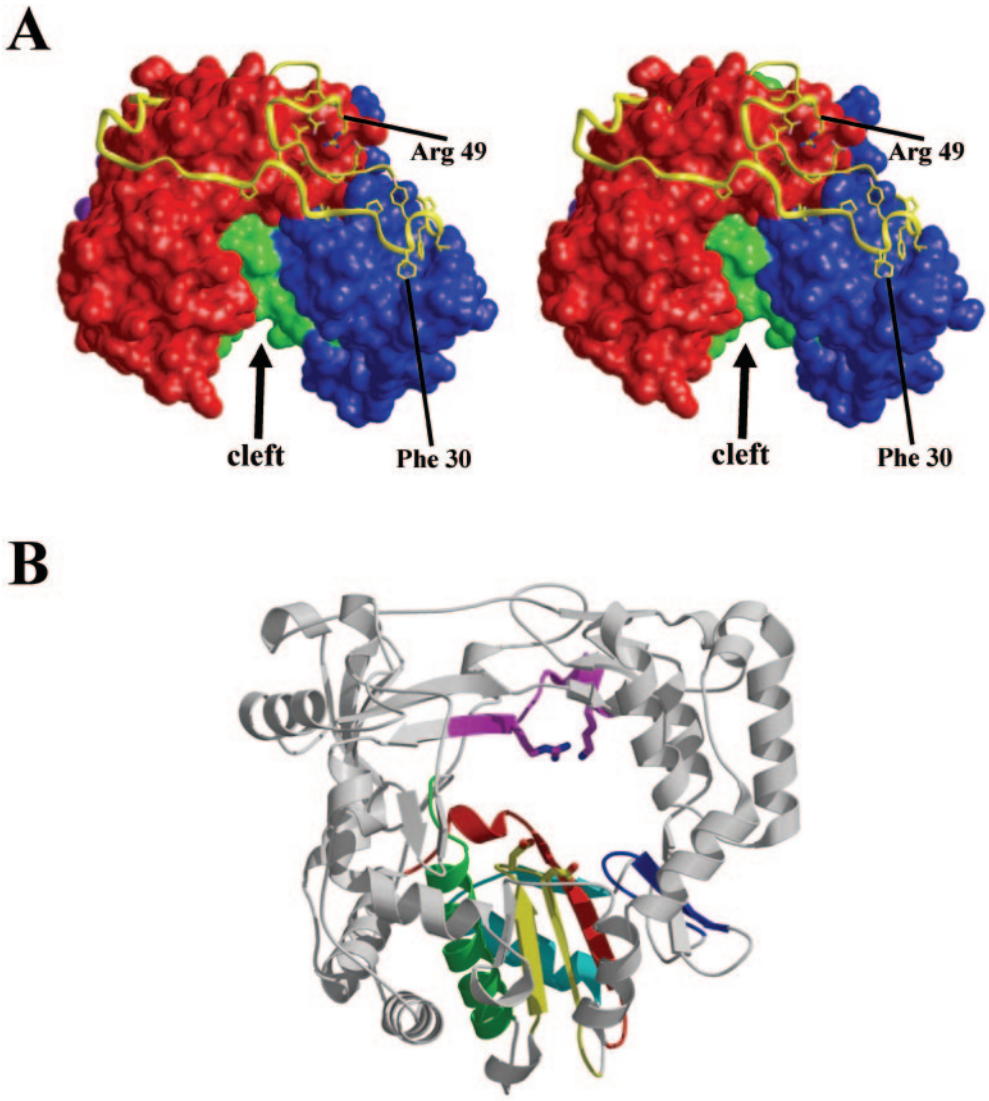

FIG. 3. (A) A stereoview of the N-terminal region tethering the fingers and thumb subdomains. The N-terminal residues (1 to 53) are shown as a yellow ribbon with selected side chains shown as stick models. The putative RNA binding cleft formed by the palm (green), fingers (red), and thumb (blue) subdomains is indicated. Phe 30 and Arg 49 are labeled for the purpose of sequence orientation. (B) The conserved polymerase structural motifs mapped onto HRV16 $3D^{pol}$. Motif A (red; residues 227 to 242), motif B (green; residues 290 to 307), motif C (yellow; residues 318 to 335), motif D (light blue; residues 227 to 242), motif E (dark blue; residues 368 to 377), and motif F (magenta; residues 167 to 176) are indicated. The putative metal binding residues (Asp 327 and Asp 328 from motif C) and the basic residues believed to interact with the rNTP (Lys 167 and Arg 174 from motif F) are indicated by stick models.

ment then folds back on itself, forming a smaller loop (residues 41 to 53), which sits at the top of the polymerase molecule and forms contacts with the tip of the fingers subdomain. The bridging of the fingers and thumb subdomains is unique to RdRps and gives them a globular shape rather than the U shape observed in the DNA polymerases, DNA-dependent RNA polymerases, and the HIV RT.

Picornaviruses are known to utilize 3CD, an uncleaved precursor of the protease and polymerase generated during polyprotein processing, as a functional intermediate in viral replication (16, 17). Interestingly, while PV 3CD contains an active $3C^{pro}$ component, the $3D^{pol}$ remains inactive until protein processing is complete (16). In light of the HRV $3D^{pol}$ structure, it is possible that the inactive polymerase results from a disruption in the N-terminal region of the protein that may occur while the polymerase is still fused to the C terminus of $3C^{pro}$. However, it is also likely that the $3C^{pro}$ molecule is simply blocking access to the active site cavity of the polymerase in 3CD. Further studies are required to determine the precise mechanism of HRV $3D^{pol}$ activation after cleavage of 3CD.

Fingers subdomain. The fingers subdomain (residues 54 to 201 and 243 to 290) of HRV16 $3D^{pol}$ consists of a five-stranded mixed β-sheet (one strand is contributed by the N-terminal region) and eight α-helices. The arrangement of secondary structures is similar to that seen in the fingers subdomains of other RdRp structures. Highlighting the topological similarity between the caliciviral RdRps and HRV16 $3D^{pol}$ is a large

loop comprised of residues 158 to 175 (172 to 189 in RHDV; 165 to 183 in NV) and an α-helix containing residues 53 to 65 (63 to 75 in RHDV; 58 to 70 in NV) which form the tips of the fingers subdomain and provide several contacts with residues from the N-terminal region. The helix-loop-helix insertion (residues 244 to 268) observed in the fingers subdomains of other viral RdRps (28) is also present. Unique to HRV16 $3D^{pol}$ is a small loop (residues 102 to 108) that is inserted after a short α-helix on the front face of the fingers subdomain (see Fig. 5C). An additional conserved structural element in RdRps, motif F, was first identified in the structure of HCV NS5B (residues 155 to 160) (28) and does have a counterpart in HRV16 $3D^{pol}$ (residues 167 to 176). Although the topology in this region of the fingers subdomain varies between the two enzymes, the positions of Lys 155 and Arg 158 of HCV NS5B, which may interact with the negatively charged phosphate groups of the incoming ribonucleotide-5′ triphosphate (rNTP), overlap very well with Lys 167 and Arg 174 of HRV16 $3D^{pol}$ (see Fig. 4B).

Palm subdomain. The palm subdomain (residues 202 to 242 and 291 to 355) is made up of a four-stranded, antiparallel core β-sheet flanked by three α-helices. Often referred to as the catalytic subdomain, the palm subdomain is rich in conserved structural motifs (Fig. 3B), and many of its features are shared across all families of RNA and DNA polymerases (15, 46, 48). Motif A (residues 229 to 239) forms a β-strand and contains a conserved aspartic acid residue (Asp 234) which is believed to contribute to nucleotidyl transfer activity by chelating metal ions associated with incoming rNTPs (2). Motif A also contains Asp 239, which may play an important role in the selection of rNTPs over 2′ deoxyribonucleotide triphosphates by hydrogen bonding to the 2′ and 3′ hydroxyl groups of the incoming nucleotide substrate (13, 28). The well-characterized Gly-Asp-Asp (Gly 326-Asp 327-Asp 328 in HRV $3D^{pol}$) sequence, conserved among the viral RdRps, is located on the turn between the two β-strands which comprise motif C (residues 322 to 333). Together with Asp 234 from motif A, these aspartic acid residues coordinate the metal ions associated with the incoming rNTP and position the triphosphate group of the nucleotide for attack by the 3′ hydroxl moiety of the primer strand (2, 47). Motif B forms an α-helix that packs against one strand of the core β-sheet and contains a conserved Asn residue (Asn 296) which has been implicated in the selection of rNTPs by hydrogen bonding to the 2′ hydroxyl moiety (12, 13). Motif D, formed by residues 338 to 353, is comprised of an α-helix and a short loop which bends back around to form the fourth β-strand of the core β-sheet located in the palm subdomain. An additional conserved structural element unique to RNA-dependent polymerases, motif E (residues 368 to 377), forms a tight loop which lies at the junction between the palm and thumb subdomains. The turn of this loop projects into the active site cavity where it has been implicated in helping to position the 3′ end of the primer strand for attack on the α-phosphate of the NTP during phosphoryl transfer (22).

Thumb subdomain. The thumb subdomain (residues 392 to 460) consists of three antiparallel α-helices followed by an extended loop segment which connects to an additional C-terminal α-helix. The NV RdRp and RHDV RdRp have topologies in their thumb subdomains that are similar to the topology of the HRV16 $3D^{pol}$ thumb subdomain, with the exception that the calicivirus polymerases have a much larger loop between the first and second α-helices. In contrast to the N-terminal region of HRV16 $3D^{pol}$, which loops over the tip of the thumb subdomain, the larger loop of the caliciviral thumb subdomains actually bends over the N-terminal region. The thumb subdomain of HRV16 $3D^{pol}$ differs considerably from that of HCV, BVDV, and Φ6 polymerases. The larger thumb subdomain of HCV NS5B contains more than twice the number of residues as HRV16 $3D^{pol}$ and includes three additional α-helices and a β-loop structure which protrudes into the active site. NV RdRp, HCV NS5B, BVDV NS5B, and the Φ6 polymerase also contain C-terminal extensions that fold back into the molecule to various degrees, filling the active site cavity. The C-terminal helix of HRV16 $3D^{pol}$ packs against the front face of the molecule, leaving the active site cavity largely exposed.

Comparisons to PV $3D^{pol}$. The structure of HRV16 $3D^{pol}$ and the known portions of PV $3D^{pol}$ (15) align very well (rmsd of 1.1 Å for 292 Cα atoms). Residues missing from the PV $3D^{pol}$ structure, presumably due to disorder in the crystal, include a majority of the N-terminal region and fingers subdomain (Fig. 2). One major difference between the two polymerase molecules occurs in 13 residues of the N-terminal region (residues 12 to 24). In the partial PV $3D^{pol}$ model these residues extend into the active site cavity. In the complete HRV16 $3D^{pol}$ structure, the N-terminal region is involved in tethering the fingers and thumb subdomains. Considering the similarities of the two polymerases in terms of sequence, structure, and function, it seems likely that these 13 residues are misfolded or modeled incorrectly in the present PV $3D^{pol}$ structure.

The topology of the thumb subdomains of HRV16 $3D^{pol}$ and PV $3D^{pol}$ are identical. Interestingly, the entire thumb subdomain of the PV $3D^{pol}$ appears to rotate by a few degrees towards the palm subdomain in comparison to its orientation in HRV16 $3D^{pol}$, suggesting that this subdomain has some conformational flexibility. In fact, when molecules A and C of the HRV16 $3D^{pol}$ ASU are aligned exclusively based on the fingers and palm subdomains (rmsd 0.7 Å for 355 Cα atoms), the 105 Cα atoms in the corresponding thumb subdomains display an rmsd of nearly 1.2 Å. This deviation appears to result from a slight rotation of the thumb subdomain of molecule A towards the palm subdomain (Fig. 4A), similar to the thumb rotation observed in the comparison of HRV16 $3D^{pol}$ and PV $3D^{pol}$. In yet another example, the two molecules which comprise the ASU of the RHDV RdRp also display roughly an 8° rotation of the N-terminal region and thumb subdomain about a similar axis (36). Although variability in the conformation of the thumb subdomains appears to be largely a result of crystal packing forces, these observations suggest that the thumb subdomains of viral RdRps may contain inherent flexibility that is constrained by an N-terminal linkage to the fingers subdomain.

The particular way that PV $3D^{pol}$ molecules pack into crystals has been used as support for a hypothesis which suggests that the polymerase forms extended oligomers in solution (15). The observation of a repeating thumb-palm interface (interface I) throughout the crystal, together with biochemical evidence for polymerase-polymerase interactions, has led to the idea that these oligomers may play a physiologically relevant roll during replication (18, 30). Crystal packing analysis of

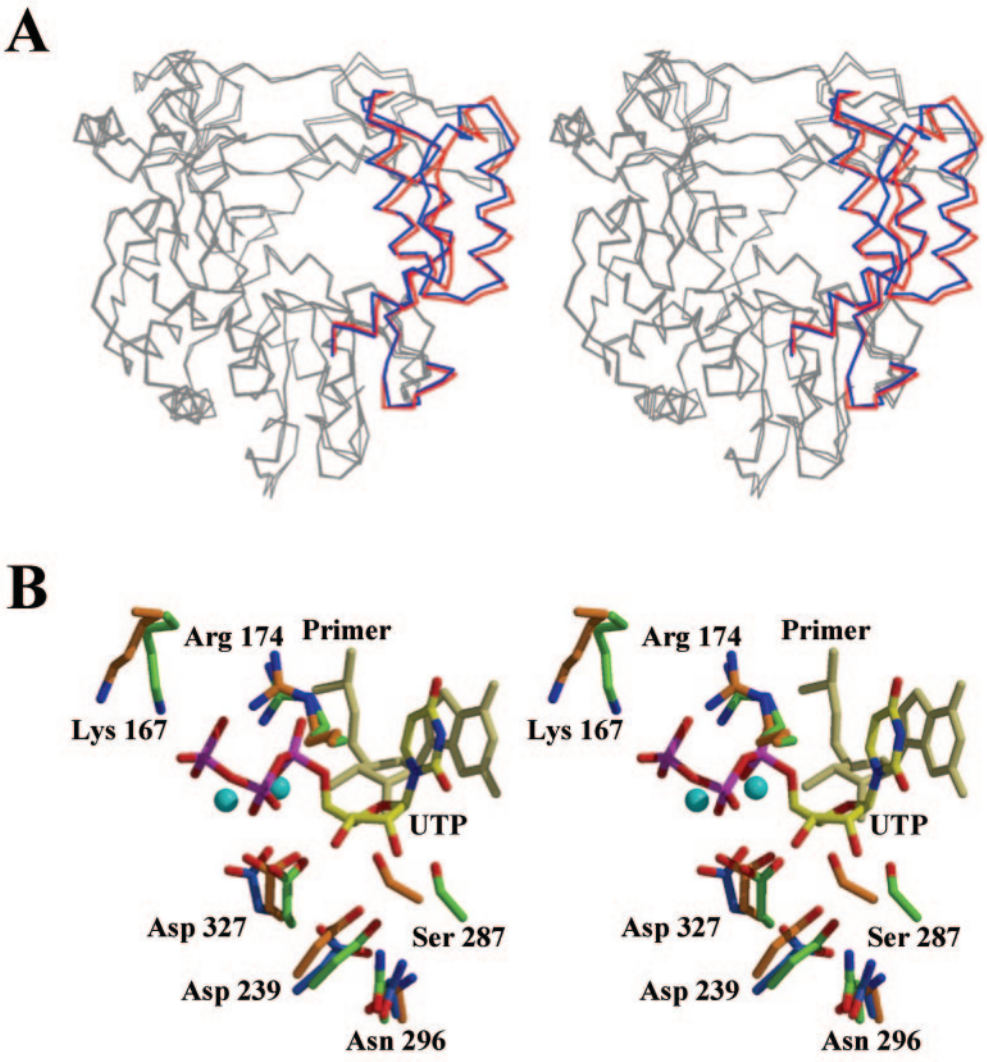

FIG. 4. (A) A stereoview of the thumb subdomain rotation observed between molecules A (blue) and C (red). The molecules were aligned exclusively by the finger and palm subdomains (gray in both molecules). (B) Active site comparison between HRV16 3D^{pol} (green sticks), PV 3D^{pol} (blue sticks), and HCV NS5B (orange sticks). UTP (yellow sticks), magnesium ions (cyan spheres), and the 3′ end of the primer strand (beige sticks) from the rough HRV16 3D^{pol}-substrate model are also included. Residues are numbered according to the HRV16 3D^{pol} sequence.

HRV16 3D^{pol} reveals that a thumb-palm interface does exist. However, a closer look at each of the four independent molecules reveals that at least two different types of interfaces exist between the thumb and palm subdomains of adjacent molecules in the ASU. The buried surface areas of the thumb-palm interface between molecules A and B and between molecules D and A′ (A′ is from a crystallographically related ASU) are 1229 and 1257 Å^2, respectively. The corresponding surface areas between molecules B and C and molecules C and D are only 793 and 826 Å^2, respectively. While the variability of this particular interface in the crystals does not exclude the possibility that HRV16 3D^{pol} forms extended oligomers in solution, it does suggest that this particular interface may simply be a result of favorable crystal packing interactions.

Hypothetical substrate modeling. In the absence of direct structural evidence relating to how the physiological substrates bind in the large, exposed active site of HRV16 3D^{pol}, the HIV RT ternary complex structure (20) was used as a guide to model a template-primer duplex and an incoming rNTP molecule. Results of similar modeling procedures have previously been reported for both RHDV 3D^{pol} and HCV NS5B (28, 36). Productive enzyme-nucleic acid complexes have been determined for both the Φ6 RdRp (5) and reovirus polymerase, λ3 (49). In both of these cases, however, a short template (less than eight nucleotides) was utilized. For our model, we were interested in observing the possible interactions of HRV16 3D^{pol} with the exiting duplex product; hence, the HIV RT ternary complex was chosen as the model. The HIV RT substrate model, including the DNA duplex, the metal ions, and the incoming nucleotide, were treated as a single rigid body during the alignment procedures.

Surprisingly, the single-stranded template, the 3′ end of the primer strand, the incoming rNTP, and the duplex product fit into the HRV16 3D^{pol} active site cavity quite well by simply

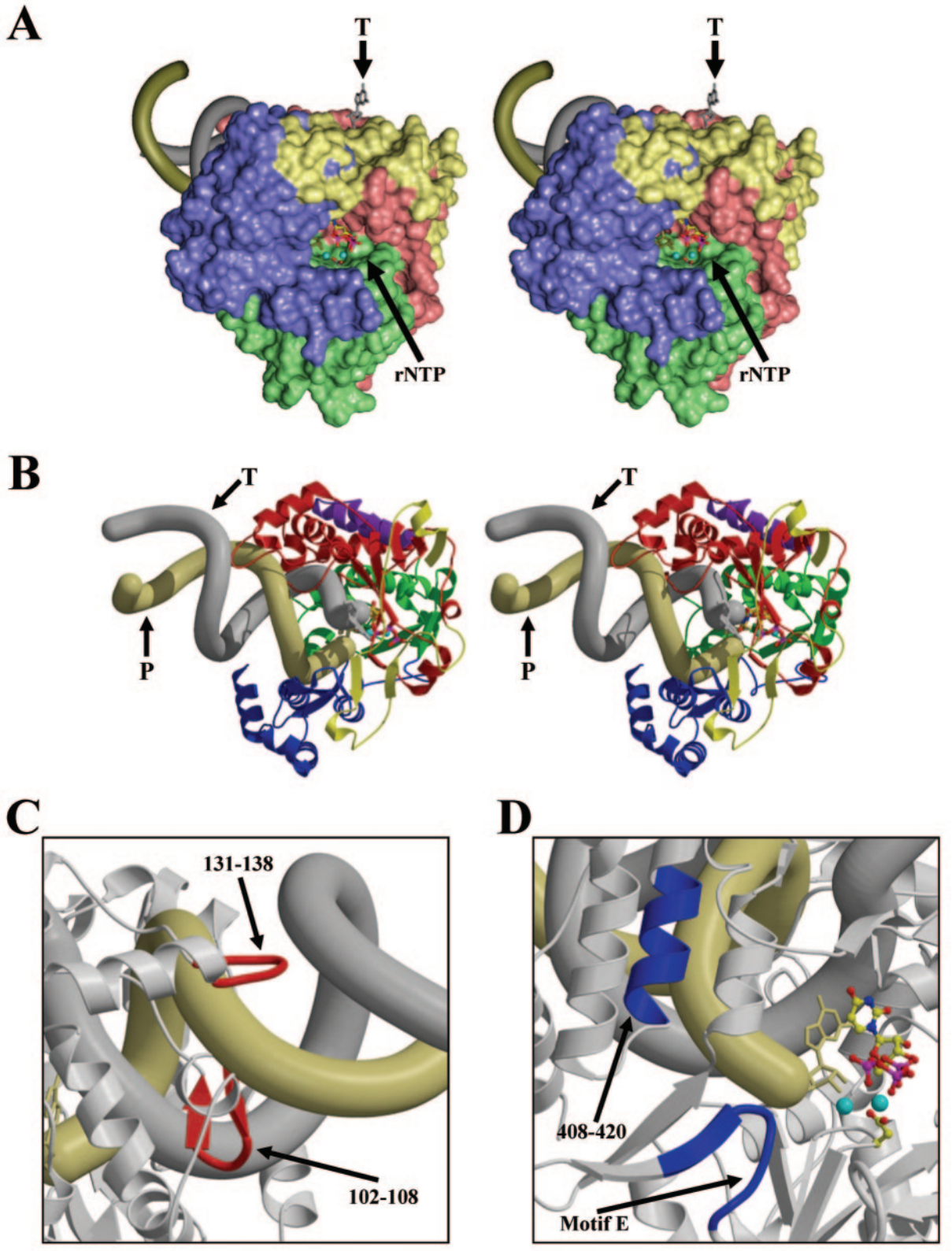

FIG. 5. Hypothetical elongation complex. (A) A stereoview of HRV16 $3D^{pol}$ structure rendered as a surface and viewed from the rear of the molecule towards the rNTP binding tunnel. The protein is colored by region according to the scheme described in the legend of Fig. 1B. The template strand (gray), primer strand (gold), UTP (stick model), and metal ions (cyan spheres) are modeled into the enzyme active site. The 5′ template (T) overhang enters from the top of the polymerase. The incoming UTP and magnesium ions are positioned above Asp 327 of motif C. (B) Stereoview looking down on top of HRV16 $3D^{pol}$. The template strand (T), primer strand (P), and protein are colored as above. (C) Two loops of the fingers subdomain (residues 102 to 108 and residues 131 to 138) may interact with the duplex product. (D) Residues (408 to 420) from the thumb subdomain and motif E may help grip the 3′ end of the primer strand.

using a few elements of the highly conserved palm subdomain as structural alignment constraints (Fig. 5). The model suggests that the duplex product is cradled by the fingers and thumb subdomains as it exits from the front of the polymerase molecule. Residues 102 to 108 and 131 to 138 of the fingers subdomain form short loops that may aid in stabilizing the elongation complex by increasing the interactions between the polymerase and the double-stranded product (Fig. 5C). In the model, the thumb subdomain is adjacent to the primer strand, where the second α-helix (residues 408 to 420) runs along the phosphodiester backbone of the primer. Residues in this helix together with motif E (residues 368 to 377), located in the junction between the palm and thumb subdomains, may help to position the 3′ end of the primer strand during RNA elongation (Fig. 5D) (22).

Extensive modeling studies based on alignments of the partial PV 3D^{pol} model and the HIV RT complex structure have been performed by Gohara et al. (13). Results from the minimized PV 3D^{pol} substrate model together with elegant kinetic and thermodynamic studies implicate specific functional roles for several residues located in the conserved motifs of the polymerase (12). Comparison of our rough HRV16 3D^{pol} substrate model to the available data from the PV 3D^{pol} modeling studies, the structure of PV 3D^{pol}, and the well-characterized structure of HCV NS5B allows us to identify several key residues in HRV16 3D^{pol} that may be involved in nucleotide binding and catalysis.

In our model, the conserved Asp 327 in motif C of HRV16 3D^{pol} (Asp 328 in PV 3D^{pol} and Asp 318 in HCV NS5B) is in a good position to bind to the magnesium ions associated with the incoming nucleotide (Fig. 4B). During nucleotidyl transfer, Asp 327 and Asp 328 from motif C, together with Asp 234 from motif A, are probably responsible for coordinating the metal ions and helping to orient the 5′ triphosphate group for nucleophillic attack by the 3′ end of the primer. The basic residues, Lys 167 and Arg 174, from motif F are also in an ideal position to interact with the negatively charged phosphates of the incoming nucleotide. These residues overlap well with Lys 155 and Arg 158 of HCV NS5B, which are reported to play a similar role in substrate binding. Although this region of the fingers subdomain is missing in the partial PV 3D^{pol} structure, homology modeling was used to predict a similar role for Lys 167 and Arg 174 (13). The carboxylate side chain of Asp 239 from motif A in our model (Asp 238 in PV 3D^{pol} and Asp 225 in HCV NS5B) is in close proximity to both the 3′ hydroxyl and 2′ hydroxyl groups of the NTP. Asp 238 from PV 3D^{pol} has been shown to play a critical role in NTP selection and binding, as well as being required for efficient phosphoryl transfer. It has also been suggested that Asn 297 from motif A in PV 3D^{pol} (Asn 296 in HRV16 3D^{pol} and Asn 291 in HCV NS5B) plays a role in the selection of rNTPs over deoxyribonucleotide triphosphates by hydrogen bonding directly to the 2′ hydroxyl group of the incoming nucleotide. In our model, it appears that Asn 296 is precluded from interacting directly the nucleotide sugar by Asp 239. After a simple side chain adjustment, the hydroxyl group of nearby Ser 287 (Ser 288 in PV 3D^{pol} and Ser 282 in HCV NS5B), however, is in an excellent position to interact with the 2′ hydroxyl group of the rNTP. Interestingly, an HCV resistant to the potent inhibitor, 2′-C-methyladenosine (7), has been characterized and contains a single Ser282Thr mutation (34). It has been shown that the phosphorylated form of this particular inhibitor is utilized as a substrate by wild-type NS5B during HCV RNA replication, where it subsequently acts as a chain terminator. The resistance seems to arise from the fact that the bulkier Thr 282 side chain selects against the 2′ methyl addition on the sugar moiety of the inhibitor, implying that this residue must be in close proximity to the 2′ position of the rNTP during catalysis. Although this region of the active site is missing in the PV 3D^{pol}, studies have suggested that the homologous Ser 288 may play a role in positioning Asp 238. The crystal structure of a picornaviral polymerase substrate ternary complex will aid greatly in assigning exact roles to key active site residues.

Structural implications for protein-primed terminal initiation. Earlier studies with PV with the two-hybrid system reveal direct evidence for binding between 3D^{pol} and VPg; however, the polymerase shows much higher affinity for 3AB, the precursor to VPg (51). Subsequent mutational analysis reveals that only mutations in the 3B sequences of 3AB disrupt the interaction with 3D^{pol}, again suggesting that VPg is responsible for direct interaction with the polymerase (51). Recent studies with PV have mapped out a region on 3D^{pol} that appears to be important for binding 3AB, for localizing 3D^{pol} to membranes, and for the uridylylation of VPg (30). Phe 377, Arg 379, and Val 391 of PV 3D^{pol} (Gly 376, Arg 378, and Thr 390 in HRV16 3D^{pol}) map to the back side of the polymerase molecule at the junction between the palm and thumb subdomains (Fig. 6A) and are believed to be essential for efficient binding of 3AB and uridylylation of VPg. If VPg is loaded on the back side of the polymerase as this evidence suggests, then translocation would pull the peptide through the NTP binding tunnel into the active site cavity. This could result in blocking access to the narrow NTP binding tunnel, which appears much larger in the partial PV 3D^{pol} model.

We propose a different mechanism based on the complete structure of HRV16 3D^{pol}. It appears that VPg can access the active site cavity from the front of the molecule through the large putative RNA binding cleft (Fig. 6). Resting against the inside of the small thumb subdomain, the N-terminal portion of VPg would project into the active site where the hydroxyl moiety of the tyrosine residue (Tyr 3 in HRV-VPg) is in good proximity to the catalytic aspartic acids (Gly-Asp-Asp in motif C). In this position, the Tyr 3 would essentially mimic the free 3′ hydroxyl of the primer strand during RNA elongation (compare Fig. 5 and 6). Such an orientation with respect to the catalytic aspartic acid residues would conserve the mechanism described for all polymerases (47). The mutational evidence implicating residues on the back side of PV 3D^{pol} may also be explained by the fact that these residues lie in and around motif E, which has been implicated in proper positioning of the primer strand during RNA synthesis. The fact that these residues lie at the hinge region of the palm and thumb subdomains may mean that they provide an important role in maintaining the structural integrity and proper functioning of the polymerase during VPg uridylylation. The crystal structure of a 3D^{pol}-VPg complex will aid greatly in elucidating the exact mechanisms of picornavirus VPg uridylylation and terminal initiation.

The fact that the PV, RHDV, and HRV RdRps contain significantly smaller thumb subdomains compared to those of HCV, BVDV, and Φ6 may reflect the different strategies that

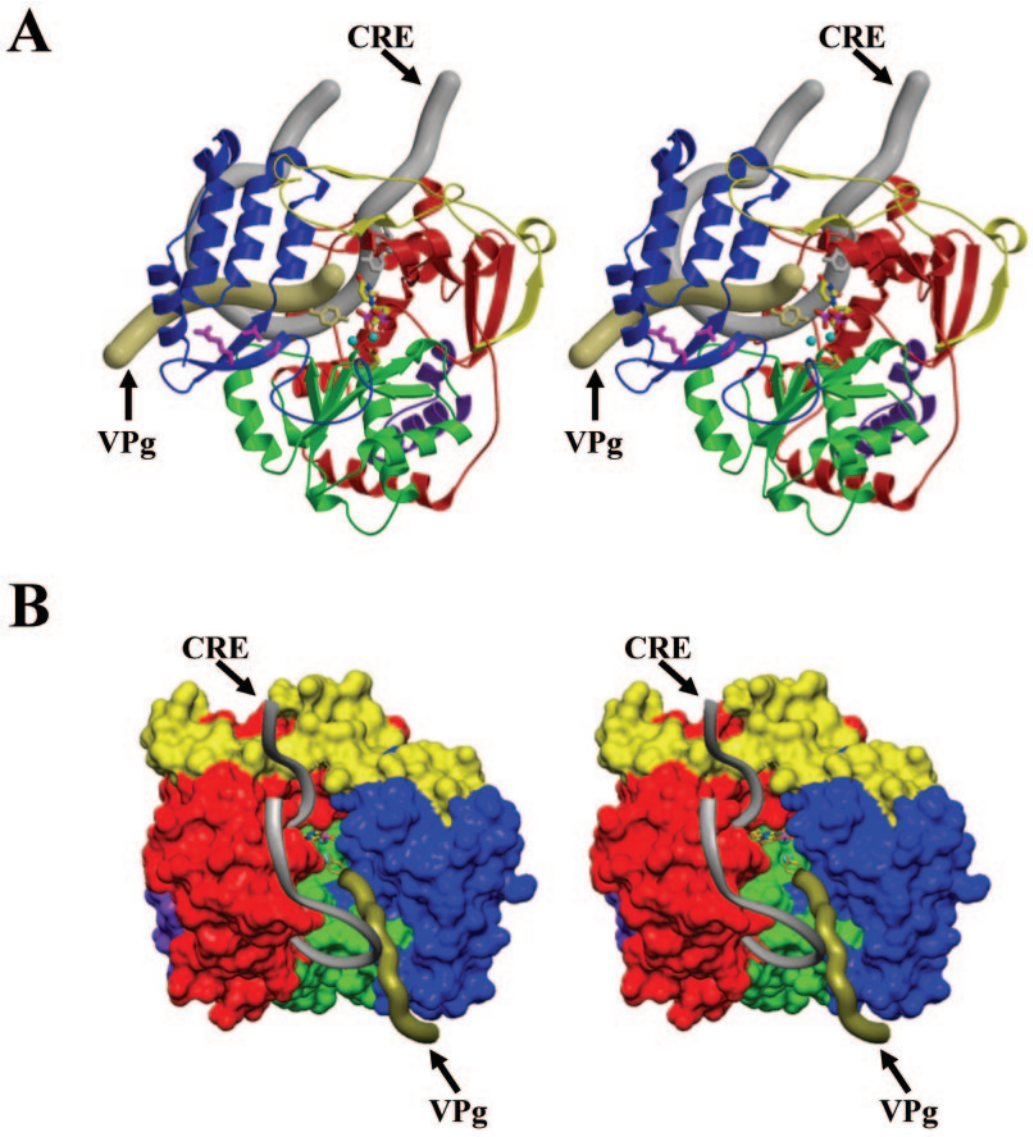

FIG. 6. Stereoviews of hypothetical VPg uridylylation. (A) Viewed from the rear of the polymerase towards the rNTP binding tunnel, the location of residues implicated in PV 3AB binding (magenta sticks) (31) are mapped onto the thumb subdomain (blue) of a ribbon representation of HRV16 $3D^{pol}$. A schematic representation of a CRE-like stem-loop (gray) and a small peptide representing VPg (gold) are modeled to illustrate the front-loading VPg uridylylation mechanism. VPg-Tyr3, UTP, and Asp 327 from HRV16 $3D^{pol}$ are represented by stick models, while the magnesium ions are shown as cyan spheres. (B) Stereoview of a surface model of VPg uridylylation. The protein model is colored according to the scheme described in the legend of Fig. 1B and is viewed looking down on the top of the polymerase. The models for CRE and VPg are colored as in panel A.

these viruses utilize to carry out terminal initiation. An RdRp with a smaller thumb subdomain may provide the room necessary to bind replication cofactors such as VPg, while a larger polymerase with an extensive thumb and C-terminal domain is capable of facilitating primer-independent terminal initiation. A similar observation was recently made by Choi et al. (9).

Summary. HRV16 $3D^{pol}$ is the enzyme responsible for nucleotidyl transferase activity during replication of the viral genome. Like other picornaviruses, HRV requires VPg, which is first uridylylated and subsequently utilized as a primer together with other viral and host cell factors in the initiation of RNA synthesis. The PV $3D^{pol}$ model, the only other structure of an RdRp from the *Picornaviridae* family to date, lacks the majority of the N-terminal region and fingers subdomain. Consequently, little structural information about the possible mechanism of VPg priming and RNA synthesis is available.

We determined the crystal structure of HRV16 $3D^{pol}$ at a 2.4-Å resolution by using both SAD phasing techniques and molecular replacement. The complete structure of HRV16 $3D^{pol}$ contains all 460 residues in addition to several solvent molecules. Consistent with other known RdRps, the fingers and thumb subdomains are tethered by the N-terminal region of the protein. Together with the palm subdomain, these structural features form a large, encircled active site cavity accessible to rNTPs through a positively charged tunnel formed on the back of the molecule. The front side of the cavity contains

a putative RNA binding cleft that can accommodate a template-primer duplex without requiring dramatic conformational changes in the protein.

Our modeling studies identify several structural elements which may be important for RNA elongation during replication of the viral genome. In addition, a front-loading mechanism for VPg uridylylation is proposed based on the presence of a small thumb domain and a large active site cavity. Because of its critical role in propagating the virus, HRV16 $3D^{pol}$ represents a potential target for antiviral therapy. The complete three-dimensional structure of HRV $3D^{pol}$ should help facilitate the design and development of direct anti-HRV agents.

ACKNOWLEDGMENTS

We thank Quan Hao and MacCHESS for arranging beam time, Meghan Reinhardt and Suhaila Naim for the protein sample preparation, and Bert L. Semler for suggestions and insight.

REFERENCES

1. **Ago, H., T. Adachi, A. Yoshida, M. Yamamoto, N. Habuka, K. Yatsunami, and M. Miyano.** 1999. Crystal structure of the RNA-dependent RNA polymerase of hepatitis C virus. Structure Fold Des. **7:**1417–1426.
2. **Beese, L. S., and T. A. Steitz.** 1991. Structural basis for the 3′-5′ exonuclease activity of *Escherichia coli* DNA polymerase I: a two metal ion mechanism. EMBO J. **10:**25–33.
3. **Blessing, R. H., and G. D. Smith.** 1999. Difference structure factor normalization for determining heavy-atom or anomalous scattering substructures. J. Appl. Cryst. **32:**664–670.
4. **Bressanelli, S., L. Tomei, A. Roussel, I. Incitti, R. L. Vitale, M. Mathieu, R. De Francesco, and F. A. Rey.** 1999. Crystal structure of the RNA-dependent RNA polymerase of hepatitis C virus. Proc. Natl. Acad. Sci. USA **96:**13034–13039.
5. **Butcher, S. J., J. M. Grimes, E. V. Makeyev, D. H. Bamford, and D. I. Stuart.** 2001. A mechanism for initiating RNA-dependent RNA polymerization. Nature **410:**235–240.
6. **Calhoun, W. J., C. A. Swenson, E. C. Dick, L. B. Schwartz, R. F. Lemanske, Jr., and W. W. Busse.** 1991. Experimental rhinovirus 16 infection potentiates histamine release after antigen bronchoprovocation in allergic subjects. Am. Rev. Respir. Dis. **144:**1267–1273.
7. **Carroll, S. S., J. E. Tomassini, M. Bosserman, K. Getty, M. W. Stahlhut, A. B. Eldrup, B. Bhat, D. Hall, A. L. Simcoe, R. LaFemina, C. A. Rutkowski, B. Wolanski, Z. Yang, G. Migliaccio, R. De Francesco, L. C. Kuo, M. MacCoss, and D. B. Olsen.** 2003. Inhibition of hepatitis C virus RNA replication by 2′-modified nucleoside analogs. J. Biol. Chem. **278:**11979–11984.
8. **Cheney, I. W., S. Naim, J. H. Shim, M. Reinhardt, B. Pai, J. Z. Wu, Z. Hong, and W. Zhong.** 2003. Viability of poliovirus/rhinovirus VPg chimeric viruses and identification of an amino acid residue in the VPg gene critical for viral RNA replication. J. Virol. **77:**7434–7443.
9. **Choi, K. H., J. M. Groarke, D. C. Young, R. J. Kuhn, J. L. Smith, D. C. Pevear, and M. G. Rossmann.** 2004. The structure of the RNA-dependent RNA polymerase from bovine viral diarrhea virus establishes the role of GTP in de novo initiation. Proc. Natl. Acad. Sci. USA **101:**4425–4430.
10. **Collaborative Computational Project, Number 4.** 1994. The CCP4 suite: programs for protein crystallography. Acta Crystallogr. Sect. D **50:**760–763.
11. **Cowtan, K.** 1994. DM: an automated procedure for phase improvement by density modification. Joint CCP4 and ESF-EACBM Newsl. Protein Crystallogr. **31:**34–38.
12. **Gohara, D. W., J. J. Arnold, and C. E. Cameron.** 2004. Poliovirus RNA-dependent RNA polymerase (3Dpol): kinetic, thermodynamic, and structural analysis of ribonucleotide selection. Biochemistry **43:**5149–5158.
13. **Gohara, D. W., S. Crotty, J. J. Arnold, J. D. Yoder, R. Andino, and C. E. Cameron.** 2000. Poliovirus RNA-dependent RNA polymerase (3Dpol): structural, biochemical, and biological analysis of conserved structural motifs A and B. J. Biol. Chem. **275:**25523–25532.
14. **Hadfield, A. T., G. D. Diana, and M. G. Rossmann.** 1999. Analysis of three structurally related antiviral compounds in complex with human rhinovirus 16. Proc. Natl. Acad. Sci. USA **96:**14730–14735.
15. **Hansen, J. L., A. M. Long, and S. C. Schultz.** 1997. Structure of the RNA-dependent RNA polymerase of poliovirus. Structure **5:**1109–1122.
16. **Harris, K. S., S. R. Reddigari, M. J. Nicklin, T. Hammerle, and E. Wimmer.** 1992. Purification and characterization of poliovirus polypeptide 3CD, a proteinase and a precursor for RNA polymerase. J. Virol. **66:**7481–7489.
17. **Harris, K. S., W. Xiang, L. Alexander, W. S. Lane, A. V. Paul, and E. Wimmer.** 1994. Interaction of poliovirus polypeptide 3CDpro with the 5′ and 3′ termini of the poliovirus genome. Identification of viral and cellular cofactors needed for efficient binding. J. Biol. Chem. **269:**27004–27014.
18. **Hobson, S. D., E. S. Rosenblum, O. C. Richards, K. Richmond, K. Kirkegaard, and S. C. Schultz.** 2001. Oligomeric structures of poliovirus polymerase are important for function. EMBO J. **20:**1153–1163.
19. **Hong, Z., C. E. Cameron, M. P. Walker, C. Castro, N. Yao, J. Y. Lau, and W. Zhong.** 2001. A novel mechanism to ensure terminal initiation by hepatitis C virus NS5B polymerase. Virology **285:**6–11.
20. **Huang, H., R. Chopra, G. L. Verdine, and S. C. Harrison.** 1998. Structure of a covalently trapped catalytic complex of HIV-1 reverse transcriptase: implications for drug resistance. Science **282:**1669–1675.
21. **Hung, M., C. S. Gibbs, and M. Tsiang.** 2002. Biochemical characterization of rhinovirus RNA-dependent RNA polymerase. Antivir. Res. **56:**99–114.
22. **Jacobo-Molina, A., J. Ding, R. G. Nanni, A. D. Clark, Jr., X. Lu, C. Tantillo, R. L. Williams, G. Kamer, A. L. Ferris, P. Clark, A. Hizi, S. H. Hughes, and E. Arnold.** 1993. Crystal structure of human immunodeficiency virus type 1 reverse transcriptase complexed with double-stranded DNA at 3.0 Å resolution shows bent DNA. Proc. Natl. Acad. Sci. USA **90:**6320–6324.
23. **Jones, T. A., J. Y. Zou, S. W. Cowan, and M. Kjeldgaard.** 1991. Improved methods for building protein models in electron density maps and the location of errors in these models. Acta Crystallogr Sect. A **47:**110–119.
24. **Kaiser, L., C. E. Crump, and F. G. Hayden.** 2000. In vitro activity of pleconaril and AG7088 against selected serotypes and clinical isolates of human rhinoviruses. Antivir. Res. **47:**215–220.
25. **Laurila, M. R., E. V. Makeyev, and D. H. Bamford.** 2002. Bacteriophage phi 6 RNA-dependent RNA polymerase: molecular details of initiating nucleic acid synthesis without primer. J. Biol. Chem. **277:**17117–17124.
26. **Lee, W. M., W. Wang, and R. R. Rueckert.** 1995. Complete sequence of the RNA genome of human rhinovirus 16, a clinically useful common cold virus belonging to the ICAM-1 receptor group. Virus Genes **9:**177–181.
27. **Leong, L. E.-C., C. T. Cornell, and B. L. Semler.** 2002. Processing determinants and functions of cleavage products of picornavirus polyproteins, p. 187–197. *In* B. L. Semler and E. Wimmer (ed.), Molecular biology of picornaviruses. American Society for Microbiology, Washington, D.C.
28. **Lesburg, C. A., M. B. Cable, E. Ferrari, Z. Hong, A. F. Mannarino, and P. C. Weber.** 1999. Crystal structure of the RNA-dependent RNA polymerase from hepatitis C virus reveals a fully encircled active site. Nat. Struct. Biol. **6:**937–943.
29. **Lu, G.** 1999. FINDNCS: A program to detect non-crystallographic symmetries in protein crystals from heavy atom sites. J. Appl. Crystallogr. **32:**365.
30. **Lyle, J. M., E. Bullitt, K. Bienz, and K. Kirkegaard.** 2002. Visualization and functional analysis of RNA-dependent RNA polymerase lattices. Science **296:**2218–2222.
31. **Lyle, J. M., A. Clewell, K. Richmond, O. C. Richards, D. A. Hope, S. C. Schultz, and K. Kirkegaard.** 2002. Similar structural basis for membrane localization and protein priming by an RNA-dependent RNA polymerase. J. Biol. Chem. **277:**16324–16331.
32. **Machin, A., J. M. Martin Alonso, and F. Parra.** 2001. Identification of the amino acid residue involved in rabbit hemorrhagic disease virus VPg uridylylation. J. Biol. Chem. **276:**27787–27792.
33. **Matthews, D. A., P. S. Dragovich, S. E. Webber, S. A. Fuhrman, A. K. Patick, L. S. Zalman, T. F. Hendrickson, R. A. Love, T. J. Prins, J. T. Marakovits, R. Zhou, J. Tikhe, C. E. Ford, J. W. Meador, R. A. Ferre, E. L. Brown, S. L. Binford, M. A. Brothers, D. M. DeLisle, and S. T. Worland.** 1999. Structure-assisted design of mechanism-based irreversible inhibitors of human rhinovirus 3C protease with potent antiviral activity against multiple rhinovirus serotypes. Proc. Natl. Acad. Sci. USA **96:**11000–11007.
34. **Migliaccio, G., J. E. Tomassini, S. S. Carroll, L. Tomei, S. Altamura, B. Bhat, L. Bartholomew, M. R. Bosserman, A. Ceccacci, L. F. Colwell, R. Cortese, R. De Francesco, A. B. Eldrup, K. L. Getty, X. S. Hou, R. L. LaFemina, S. W. Ludmerer, M. MacCoss, D. R. McMasters, M. W. Stahlhut, D. B. Olsen, D. J. Hazuda, and O. A. Flores.** 2003. Characterization of resistance to nonobligate chain-terminating ribonucleoside analogs that inhibit hepatitis C virus replication in vitro. J. Biol. Chem. **278:**49164–49170.
35. **Musher, D. M.** 2003. How contagious are common respiratory tract infections? N. Engl. J. Med. **348:**1256–1266.
36. **Ng, K. K., M. M. Cherney, A. L. Vazquez, A. Machin, J. M. Alonso, F. Parra, and M. N. James.** 2002. Crystal structures of active and inactive conformations of a caliciviral RNA-dependent RNA polymerase. J. Biol. Chem. **277:**1381–1387.
37. **Ng, K. K., N. Pendas-Franco, J. Rojo, J. A. Boga, A. Machin, J. M. Alonso, and F. Parra.** 2004. Crystal structure of Norwalk virus polymerase reveals the carboxyl terminus in the active site cleft. J. Biol. Chem. **279:**16638–16645.
38. **O'Farrell, D., R. Trowbridge, D. Rowlands, and J. Jager.** 2003. Substrate complexes of hepatitis C virus RNA polymerase (HC-J4): structural evidence for nucleotide import and de novo initiation. J. Mol. Biol. **326:**1025–1035.
39. **Otwinowski, Z.** 1991. Maximum likelihood refinement of heavy atom parameters, p. 80–85. *In* W. Wolf, P. R. Evans, and A. G. W. Leslie (ed.), Isomor-

phous replacement and anomalous scattering. Proceedings of the Daresbury Study Weekend. SERC Daresbury Laboratory, Warrington, United Kingdom.
40. **Paul, A. V., J. Peters, J. Mugavero, J. Yin, J. H. van Boom, and E. Wimmer.** 2003. Biochemical and genetic studies of the VPg uridylylation reaction catalyzed by the RNA polymerase of poliovirus. J. Virol. **77:**891–904.
41. **Paul, A. V., J. Yin, J. Mugavero, E. Rieder, Y. Liu, and E. Wimmer.** 2003. A "slide-back" mechanism for the initiation of protein-primed RNA synthesis by the RNA polymerase of poliovirus. J. Biol. Chem. **278:**43951–43960.
42. **Racaniello, V. R., and D. Baltimore.** 1981. Molecular cloning of poliovirus cDNA and determination of the complete nucleotide sequence of the viral genome. Proc. Natl. Acad. Sci. USA **78:**4887–4891.
43. **Rieder, E., A. V. Paul, D. W. Kim, J. H. van Boom, and E. Wimmer.** 2000. Genetic and biochemical studies of poliovirus *cis*-acting replication element *cre* in relation to VPg uridylylation. J. Virol. **74:**10371–10380.
44. **Rossmann, M. G., E. Arnold, J. W. Erickson, E. A. Frankenberger, J. P. Griffith, H. J. Hecht, J. E. Johnson, G. Kamer, M. Luo, and A. G. Mosser.** 1985. Structure of a human common cold virus and functional relationship to other picornaviruses. Nature **317:**145–153.
45. **Schwede, T., J. Kopp, N. Guex, and M. C. Peitsch.** 2003. SWISS-MODEL: An automated protein homology-modeling server. Nucleic Acids Res. **31:** 3381–3385.
46. **Sousa, R.** 1996. Structural and mechanistic relationships between nucleic acid polymerases. Trends Biochem. Sci. **21:**186–190.
47. **Steitz, T. A.** 1998. A mechanism for all polymerases. Nature **391:**231–232.
48. **Steitz, T. A., S. J. Smerdon, J. Jager, and C. M. Joyce.** 1994. A unified polymerase mechanism for nonhomologous DNA and RNA polymerases. Science **266:**2022–2025.
49. **Tao, Y., D. L. Farsetta, M. L. Nibert, and S. C. Harrison.** 2002. RNA synthesis in a cage—structural studies of reovirus polymerase lambda3. Cell **111:**733–745.
50. **Weeks, C. M., and R. Miller.** 1999. The design and implementation of *SnB* version 2.0. J. Appl. Cryst. **32:**120–124.
51. **Xiang, W., A. Cuconati, D. Hope, K. Kirkegaard, and E. Wimmer.** 1998. Complete protein linkage map of poliovirus P3 proteins: interaction of polymerase $3D^{pol}$ with VPg and with genetic variants of 3AB. J. Virol. **72:**6732–6741.
52. **Yang, Y., R. Rijnbrand, K. L. McKnight, E. Wimmer, A. Paul, A. Martin, and S. M. Lemon.** 2002. Sequence requirements for viral RNA replication and VPg uridylylation directed by the internal *cis*-acting replication element (*cre*) of human rhinovirus type 14. J. Virol. **76:**7485–7494.